2017

Mixed-Component Sulfone-Sulfoxide Tagged Zinc IRMOFs: In Situ Ligand Oxidation, Carbon Dioxide, and Water Sorption Studies

Macguire Bryant
University of Wollongong, mrb940@uowmail.edu.au

Andrew D. Burrows
University of Bath, a.d.burrows@bath.ac.uk

Cameron Kepert
University of Sydney, cameron.kepert@sydney.edu.au

Peter Southon
University of Sydney

Omid Qazvini
Massey University

See next page for additional authors

Publication Details

Bryant, M. R., Burrows, A. D., Kepert, C. J., Southon, P. D., Qazvini, O. T., Telfer, S. G. & Richardson, C. (2017). Mixed-Component Sulfone-Sulfoxide Tagged Zinc IRMOFs: In Situ Ligand Oxidation, Carbon Dioxide, and Water Sorption Studies. Crystal Growth and Design, 17 (4), 2016-2023.

Mixed-Component Sulfone-Sulfoxide Tagged Zinc IRMOFs: In Situ Ligand Oxidation, Carbon Dioxide, and Water Sorption Studies

Abstract

Reported here are the syntheses and adsorption properties of a series of single- and mixed-component zinc IRMOFs derived from controlled ratios of sulfide and sulfone functionalized linear biphenyldicarboxylate (bpdc) ligands. During MOF synthesis the sulfide moieties undergo in situ oxidation, giving rise to sulfoxide functionalized ligands, which are incorporated to give mixed-component sulfoxide-sulfone functionalized MOFs. The single- and mixed-component systems all share the IRMOF-9 structure type as determined by a combination of single crystal and powder X-ray diffraction analyses. The functionalized IRMOF-9 series was investigated by N_2, CO_2, and water adsorption measurements. MOFs containing higher proportions of sulfoxide have slightly larger accessible surface areas and pore volumes, whereas MOFs containing a greater proportion of the sulfone functionality demonstrated higher CO_2 adsorption capacities, enthalpies of CO_2 adsorption, and CO_2/N_2 selectivities. Water adsorption studies at 298 K showed the MOFs to have pore-filling steps starting around 0.4 P/P_0. In general, only small changes in water adsorption were observed with regards to ligand ratios in the mixed-component MOFs, suggesting that the location of the step is primarily determined by the pore size. A ligand-directed fine-tuning approach of changing alkyl chain length was demonstrated to give smaller more hydrophobic pores with better adsorption characteristics.

Disciplines

Medicine and Health Sciences | Social and Behavioral Sciences

Publication Details

Bryant, M. R., Burrows, A. D., Kepert, C. J., Southon, P. D., Qazvini, O. T., Telfer, S. G. & Richardson, C. (2017). Mixed-Component Sulfone-Sulfoxide Tagged Zinc IRMOFs: In Situ Ligand Oxidation, Carbon Dioxide, and Water Sorption Studies. Crystal Growth and Design, 17 (4), 2016-2023.

Authors

Macguire Bryant, Andrew D. Burrows, Cameron Kepert, Peter Southon, Omid Qazvini, Shane Telfer, and Christopher Richardson

Mixed-component sulfone–sulfoxide tagged zinc IRMOFs: *In situ* ligand oxidation, carbon dioxide and water sorption studies

Macguire R. Bryant[†], *Andrew D. Burrows*[‡], *Cameron J. Kepert*[§], *Peter D. Southon*[§], *Omid T. Qazvini*[‖], *Shane G. Telfer*[‖], *and Christopher Richardson*[†]*

[†]School of Chemistry, University of Wollongong, Northfields Avenue, Wollongong NSW 2522, Australia

[‡]Department of Chemistry, University of Bath, Claverton Down, Bath BA2 7AY, United Kingdom

[§] School of Chemistry, University of Sydney, Sydney NSW 2006, Australia

[‖] MacDiarmid Institute for Advanced Materials and Nanotechnology, Institute of Fundamental Sciences, Massey University, Palmerston North, New Zealand

ABSTRACT

Reported here are the syntheses and adsorption properties of a series of single- and mixed-component zinc IRMOFs derived from controlled ratios of sulfide and sulfone functionalized linear biphenyldicarboxylate (bpdc) ligands. During MOF synthesis the sulfide moieties undergo *in situ* oxidation, giving rise to sulfoxide functionalized ligands which are incorporated to give mixed-component sulfoxide-sulfone functionalized MOFs. The single-

and mixed-component systems all share the IRMOF-9 structure type as determined by a combination of single crystal and powder X-ray diffraction analyses. The functionalized IRMOF-9 series was investigated by N_2, CO_2 and water adsorption measurements. MOFs containing higher proportions of sulfoxide have slightly larger accessible surface areas and pore volumes, whereas MOFs containing a greater proportion of the sulfone functionality demonstrated higher CO_2 adsorption capacities, enthalpies of CO_2 adsorption and CO_2/N_2 selectivities. Water adsorption studies at 298 K showed the MOFs to have pore-filling steps starting around 0.4 P/P_0. In general, only small changes in water adsorption were observed with regards to ligand ratios in the mixed-component MOFs, suggesting that the location of the step is primarily determined by the pore size. A ligand-directed fine-tuning approach of changing alkyl chain length was demonstrated to give smaller more hydrophobic pores with better adsorption characteristics.

INTRODUCTION

Metal-organic frameworks (MOFs) are porous crystalline materials with promise in applications such as heterogeneous catalysis,[1-2] chemical sensing[3] and molecular separations.[4-6] Research into MOFs is developing rapidly because of their potential to tune the size and shape[7-8] and chirality[9-12] of their pores. Additionally, the chemical properties of the pore surfaces can be rationally engineered via modular synthetic methods.[13-17] This grants a great deal of control over the pore characteristics of the MOF through judicious choice of organic ligands and metal centers.[8, 15, 18]

The adsorption of gases by MOFs has seen a large amount of interest,[19-20] particularly the selective adsorption of CO_2 for carbon capture and remediation applications.[19, 21] One strategy is to use functional groups attached to the bridging ligands as sites for strong and selective binding of CO_2,[22] and a clear trend is an increase in CO_2 binding strength with increasing polarizability of the groups.[23-25] However, these types of functional groups also

tend to interact strongly with water. In situations where CO_2 and water might be found together, such as in flue gas streams, this would lead to competitive adsorption.[26-28] Further, many MOFs degrade upon contact with water.[29-31] This means a critical marker for the application of MOFs is their stability towards humid gases.[32] Also, the relative humidity at which pore-filling occurs defines a useful working range for MOFs as removal of the pore-water can stress frameworks to collapse.[32-35] Therefore, fashioning pore surfaces to repel water while maintaining favorable properties for adsorbing CO_2 is an important goal.[19, 36] Strategies to enhance the stability of MOFs towards water include functionalization of the pore space with fluorine-containing groups and alkyl chains, [37-39] and by ligand rigidification.[40-42]

One approach to chemically fine tune MOFs is by forming mixed-component MOFs (MC-MOFs; also known as multivariate or MTV-MOFs), where structurally similar, yet differently functionalized ligands, are incorporated into the lattice.[43-46] We have shown that the compositions of MC-IRMOF-1-type frameworks can be controlled by the reaction time.[45] Moreover, this approach offers the potential to tune the properties of the materials. For example, adsorption of H_2, CO_2 and CO are enhanced by combining allyloxy- and benzyloxy- functionalities in MC-IRMOF-1-type frameworks.[46] Differences in CO_2 and water adsorption were shown to depend on bdc/bdc-NH_2/bdc-NO_2 linker proportions in MC-MIL-101(Cr) MOFs.[47-48] In bpy-pillared zinc isophthalate MC-MOFs, the ratios of methoxy- and nitro-functionalized ligands could be tuned to improve the adsorption of CH_4 over CO_2 and C_2H_6.[49] Interestingly, while MC-MOFs can engender differences in properties, the responses are not always products of linear combinations of the linker components. For example, the best H_2 adsorption performance of bdc/bdc-OMe MC-IRMOF-1 was with 25% bdc-OMe incorporation[50] and the highest surface area of bdc/bdc-NH_2 MC-IRMOF-1/3 frameworks was achieved with 25% bdc-NH_2.[51] The complex nature yet clear potential to

create superior materials through a MC approach is an aspect of MOF chemistry which requires additional research.

In previous work we found that zinc MOFs made from thioether-tagged ligand $H_2\mathbf{L^1}$ and sulfone-tagged ligand $H_2\mathbf{L^2}$ (Chart 1) share an interpenetrated ***pcu*** topology akin to IRMOF-9.[52] More recently we investigated the sulfoxide-tagged ligand $\mathbf{L^3}$ in an IRMOF-9 type framework for its thermally-induced post-synthetic elimination chemistry.[53] Here we report a series of MC-IRMOF-9 compounds starting from controlled proportions of relatively non-polar sulfide and polar sulfone groups, and the influence of the chemical functional groups on CO_2 and water adsorption properties. We were particularly interested in the impact of the chemical functionality on the pore filling step in water adsorption isotherms as this is a critical measure for MOFs. We show how flexible tethers containing polar functional groups together with short alkyl chains could strike the right balance between good interactions with CO_2 and pore hydrophobicity. MOFs containing sulfide ligands have previously been shown to be relatively hydrophobic,[54] while sulfone-containing MOFs have good CO_2 binding properties.[25, 55-56] Similarly, the sulfone group is also widely used for CO_2 capture in polymers and membrane materials.[57-58]

Chart 1. Structures of ligands $H_2\mathbf{L^{1-4}}$.

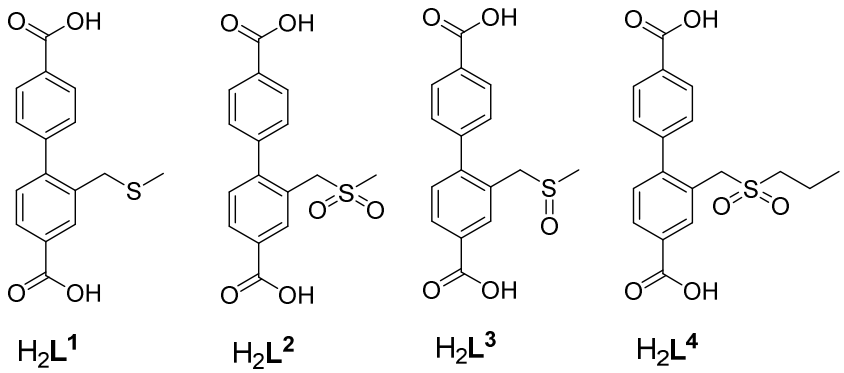

EXPERIMENTAL METHODS

MOFs MSO_2Me-15 and MSO_2Me-100 (frameworks are denoted MSO_2Me-X, where X represents the percentage of sulfone ligand $\mathbf{L^2}$ in the structure) were prepared as reported in the literature.[52-53] All chemicals used were of analytical grade and purchased from either Sigma Aldrich, VWR Australia or Ajax Finechem Pty Ltd. ^{1}H NMR and ^{13}C NMR spectra were obtained using a Varian Mercury VX-300-MHz NMR spectrometer operating at 300 MHz for ^{1}H and 75.5 MHz for ^{13}C, or a Varian Inova-500-MHz NMR spectrometer, operating at 500 MHz for ^{1}H and 125 MHz for ^{13}C. ^{1}H NMR spectra were referenced to the residual *protio* peaks at δ 2.50 ppm (d_6-DMSO) or δ 7.27 ppm in $CDCl_3$. ^{13}C NMR spectra were referenced to the solvent peaks at δ 39.6 ppm in d_6-DMSO or δ 77.7 ppm in $CDCl_3$. For ^{1}H NMR analysis, MOF samples (~10 mg) were digested by adding 35% DCl in D_2O (2 μL) and d_6-DMSO (500 μL) and stirring until a solution was obtained.

Simultaneous thermogravimetric and differential thermal analysis (TG-DTA) data were obtained using a Shimadzu DTG-60 instrument fitted with a FC-60A flow rate controller and TA-60WS thermal analyzer. Measuring parameters of 10 °C per min under nitrogen flow (20 cm^3 min^{-1}) were used. Powder X-ray diffraction (PXRD) patterns were recorded on a GBC-MMA X-ray diffractometer using Cu K(α) radiation (1.5418 Å) with samples mounted on 1" SiO_2 substrates. Experimental settings in the 2θ angle range of 3–30° of 0.04° step size and a scan speed of 3° min^{-1} were used.

Single crystal X-ray diffraction (SCXRD) data were recorded on a Rigaku Spider diffractometer equipped with a MicroMax MM007 rotating anode generator (Cu radiation, 1.54180 Å), fitted with high flux Osmic multilayer mirror optics, and a curved image-plate detector. Data were collected at 293 K and were integrated and scaled and averaged with FS process.[59] XPREP was used to determine the space group and the structure was solved using SHELXS and refined with SHELXL.[60] Details on the refinement can be found in the SI to

this article. Data are deposited with the Cambridge Structural Database (CCDC 1503491). Data can be obtained for free from www.ccdc.cam.ac.uk

Gas adsorption studies up to 1 bar were carried out using a Quantachrome Autosorb MP instrument and high purity nitrogen (99.999 %) and carbon dioxide (99.995 %) gases at the Wollongong Isotope Geochemistry Laboratory. Surface areas were determined using Brunauer-Emmett-Teller (BET) calculations. Pore size distributions were calculated using the QSDFT kernel for N_2 at 77 K on carbon with slit/cylindrical pores as implemented in the Quantachrome software (v 3.0). Vapor and gas adsorption studies up to 10 bar were carried out on a Hiden Isochema IGA-002 Single Component Gas and Vapor Adsorption Analyzer. The enthalpy of adsorption as a function of CO_2 loading was calculated by application of the Clausius-Clapeyron equation to CO_2 isotherms measured at 273 K, 288 K and 298 K; the isotherms were interpolated by fitting a cubic spline to the data. Elemental microanalysis was performed by the Microanalytical Unit at the Australian National University using a Carlo Erba 1106 automatic analyzer, and the Elemental Microanalysis Service at Macquarie University using a PerkinElmer Elemental Analyzer, Model PE2400 CHNS/O. Each sample was heated at 110 °C for 2 h and analyzed immediately afterward.

Synthetic procedure for H_2L^4

Synthesis of dimethyl 2-((propylthio)methyl)-[1,1'-biphenyl]-4,4'-dicarboxylate

Propanethiol (200 μL, 2.2 mmol) and then Et_3N (150 μL, 1.1 mmol) were added to dimethyl 2-(bromomethyl)-[1,1'-biphenyl]-4,4'-dicarboxylate (278 mg, 0.76 mmol) in CH_2Cl_2 (3 cm^3) with stirring. After 5 days the reaction was worked up by dilution with CH_2Cl_2 (5 cm^3) washing with aqueous NaOH (0.25 M), brine, drying over Na_2SO_4 and rotary evaporation. The residue was assayed by NMR spectroscopy and showed only product (R_f 0.82, 1–1 CH_2Cl_2–Hexane). ^{1}H NMR δ_H/ppm (500 MHz; $CDCl_3$) 0.90 (3 H, t, J = 7.25 Hz), 1.47 (2 H, q, J = 7.25 Hz), 2.38 (2 H, t, J = 7.25 Hz), 3.67 (2H, s), 3.96 (6 H, s), 7.31 (1 H, d,

J = 8.00 Hz), 7.51 (2 H, d, *J* = 8.00 Hz), 7.96 (1 H, d, *J* = 8.00 Hz), 8.13 (3 H, m). ^{13}C NMR δ_C/ppm (125 MHz; $CDCl_3$) 14.04, 23.26, 34.46, 35.18, 52.89, 127.92, 128.77, 129.86, 130.18, 130.22, 130.54, 130.86, 132.20, 137.07, 145.51, 146.12, 167.34, 167.50.

Synthesis of dimethyl 2-((propylsulfonyl)methyl)-[1,1'-biphenyl]-4,4'-dicarboxylate

The residue obtained above was taken up in AcOH (3 cm^3) and 30% H_2O_2 (0.5 cm^3, 4.4 mmol) was added drop wise with stirring. The mixture was heated to 80 ºC for one hour and after cooling most of the AcOH was removed by rotary evaporation. The product was precipitated by the addition of water, separated by filtration, washed with water, air dried, and crystallized from MeOH/H_2O (R_f 0.35, 1–1 CH_2Cl_2–Hexane). ^{1}H NMR δ_H/ppm (500 MHz; $CDCl_3$) 0.95 (3 H, t, *J* = 7.50 Hz), 1.62 (2 H, m), 2.70 (2 H, t, *J* = 8.00 Hz), 3.96 (6 H, s), 4.28 (2 H, s), 7.41 (1 H, d, *J* = 8.00 Hz), 7.47 (2 H, d, *J* = 8.00 Hz), 8.11 (1 H, d, *J* = 5.00 Hz), 8.15 (2 H, d, *J* = 5.00 Hz), 8.32 (1 H, s). ^{13}C NMR δ_C/ppm (125 MHz; $CDCl_3$) 13.69, 16.34, 53.00, 53.08, 55.17, 56.02, 126.25, 130.07, 130.60, 130.70, 130.73, 131.04, 131.42, 133.64, 144.59, 147.59, 166.82, 167.23.

Synthesis of 2-((propylsulfonyl)methyl)-[1,1'-biphenyl]-4,4'-dicarboxylic acid (H_2L^4)

1M NaOH solution (0.690 cm^3, 0.690 mmol) was added dropwise to dimethyl 2-((propylsulfonyl)methyl)-[1,1'-biphenyl]-4,4'-dicarboxylate (107.65 mg, 0.276 mmol) dissolved in MeOH (5.5 cm^3) and THF (1 cm^3) and left to stir for 18 hours. The solution was filtered and the MeOH and THF were removed by rotary evaporation before dilution with water (10 cm^3) and acidification with 1M HCl. The precipitated solid was separated by filtration, washed with water (3 × 10 cm^3), and air dried overnight. Yield = 87.3 mg (86 %). ^{1}H NMR δ_H/ppm (500 MHz; *d*$_6$-DMSO) 0.84 (3 H, t, *J* = 7.50 Hz), 1.56 (2 H, m), 2.90 (2 H, t, *J* = 7.50 Hz), 4.45 (2 H, s), 7.46 (1 H, d, *J* = 8.00 Hz), 7.54 (2 H, d, *J* = 7.50 Hz), 8.02 (3 H, m), 8.15 (1 H, s), 13.12 (2 H s). ^{13}C NMR δ_C/ppm (125 MHz; *d*$_6$-DMSO) 12.71, 15.40, 54.11,

126.07, 129.34, 129.48, 129.53, 129.77, 130.18, 130.22, 130.51, 130.97, 133.60 (br), 143.60, 146.56, 166.79, 167.11.

General synthetic procedure for MSO_2Me-36, MSO_2Me-64, MSO_2Me-79

The requisite amounts of $Zn(NO_3)_2{\cdot}6H_2O$, $H_2\mathbf{L^1}$ and $H_2\mathbf{L^2}$ were stirred in *N,N′*-dimethylformamide (DMF) (16 cm^3) until a solution was obtained. The solution was placed in an oven pre-heated to 100 ºC for 24 hours. The DMF solution was then exchanged three times for fresh DMF (2 cm^3) at 100 °C, then at room temperature for CH_2Cl_2 over 3 days, and then for benzene over 2 days. The samples were activated by freeze drying at –53 °C and 0.09 mbar for 1 hour followed by heating under dynamic vacuum at 120 °C for 5 hours.

Data for MSO_2Me-36 (WUF-7; WUF, Wollongong University Framework)

$Zn(NO_3)_2{\cdot}6H_2O$ (267.0 mg, 0.897 mmol), $H_2\mathbf{L^1}$, (67.8 mg, 0.224 mmol), $H_2\mathbf{L^2}$ (25.0 mg, 0.075 mmol); Yield 49 %; Elemental analysis of MSO_2Me-36 $[Zn_4O(\mathbf{L^2})_{1.08}(\mathbf{L^3})_{1.92}(H_2O)_{0.75}]$: calc. C: 45.86%, H: 3.01%, S: 7.63%, N: 0.00%; Found C: 46.10%, H: 3.28%, S: 6.76%, N: 0.00%.

Data for MSO_2Me-64 (WUF-8)

$Zn(NO_3)_2{\cdot}6H_2O$ (294 mg, 0.987 mmol), $H_2\mathbf{L^1}$ (49.8 mg, 0.165 mmol), $H_2\mathbf{L^2}$ (55.2 mg (0.165 mmol); Yield 56 %; Elemental analysis of MSO_2Me-65 $[Zn_4O(\mathbf{L^2})_{1.92}(\mathbf{L^3})_{1.08}(H_2O)_2]$: calc. C: 44.59%, H: 3.12%, S: 7.42%, N: 0.00%, Found C: 44.12%, H: 3.09%, S: 7.26%, N: 0.00%

Data for MSO_2Me-79 (WUF-9)

$Zn(NO_3)_2{\cdot}6H_2O$ (266.8 mg, 0.897 mmol), $H_2\mathbf{L^1}$ (22.6 mg, 0.075 mmol), $H_2\mathbf{L^2}$ (75.0 mg, 0.224 mmol); Yield 60 %; Elemental analysis of MSO_2Me-79 $[Zn_4O(\mathbf{L^2})_{2.38}(\mathbf{L^3})_{0.62}(H_2O)_2]$: calc. C: 44.34%, H: 3.10%, S: 7.38%, N: 0.00%, Found C: 44.12%, H: 3.09%, S: 7.26%, N: 0.00%.

Synthetic procedure for MSO_2Pr-100 (WUF-10)

$Zn(NO_3)_2 \cdot 6H_2O$ (70.5 mg, 0.237 mmol) and $H_2\mathbf{L^4}$ (28.7 mg, 0.079 mmol) were stirred in DMF (4 cm^3) until a solution was obtained. The solution was placed in an oven pre-heated to 100 ºC for 24 hours. The crystals were treated in the same manner as in the general procedure. Elemental analysis of MSO_2Pr-100 [$Zn_4O(\mathbf{L^4})_3(H_2O)$]: calc. C: 47.12%, H: 3.66%, S: 6.97%, N: 0.00%, Found C: 47.07%, H: 3.41%, S: 6.71%, N: 0.00%.

RESULTS

Synthesis and Characterization

A series of five functionalized MC-IRMOF-9 analogues containing $\mathbf{L^2}$ and $\mathbf{L^3}$ (denoted MSO_2Me-X, where X represents the percentage of sulfone ligand $\mathbf{L^2}$ in the structure) were prepared by direct solvothermal syntheses reacting $Zn(NO_3)_2 \cdot 6H_2O$ with defined ratios of $H_2\mathbf{L^{1\text{-}3}}$ (Table 1) over 24 hours in DMF at 100 ºC. Single-component MSO_2Pr-100 was prepared similarly by direct solvothermal synthesis from $Zn(NO_3)_2 \cdot 6H_2O$ and $H_2\mathbf{L^4}$. In order to determine the proportions of each ligand in the MC-MOFs, samples were solvent exchanged and activated before digestion in DCl and *d*$_6$-DMSO for analysis using ^{1}H NMR spectroscopy. The spectra show no $\mathbf{L^1}$ is present in the MC-MOFs (Figure 1) as the characteristic methyl (δ 1.91 ppm) and methylene signals (δ 3.71 ppm) for this compound are absent. Instead, the presence of the sulfoxide-tagged ligand $\mathbf{L^3}$ (Chart 1) is confirmed by the appearance of doublets at δ 4.03 and δ 4.15 ppm for the methylene protons. This indicates that during MC-MOF synthesis, $H_2\mathbf{L^1}$ is completely converted to $H_2\mathbf{L^3}$ by oxidation. The ^{1}H NMR data was used to calculate the relative incorporation of the ligands in the MC MOFs, allowing the compositions of the frameworks to be formulated (Table 1).

We have previously reported MSO_2Me-15 (WUF-6), which although being prepared solely from sulfoxide ligand $H_2\mathbf{L^3}$ contains 15% of the sulfone $\mathbf{L^2}$ in its structure. We ascribed this to occur *via* disproportionation–re-oxidation pathways during MOF synthesis.[53] Considering this result, the increased incorporation of $\mathbf{L^2}$ into MSO_2Me-36, MSO_2Me-64 and MSO_2Me-

79 relative to the starting synthetic ratio arises from the *in situ* oxidation chemistry, rather than *via* a selective incorporation of $\mathbf{L^2}$ over $\mathbf{L^1}$/$\mathbf{L^3}$.

Table 1. Starting synthetic ratios, percentage compositions and framework formulations of the MOFs synthesized in this work.

MOF	*H_2L^2 : H_2L^1 synthesis ratio (mol%)*	*Ligand incorporation in MOF (mol%)*[a]		*Framework Formulation*
		$\mathbf{L^2}$	$\mathbf{L^3}$	
MSO_2Me-15	-[b]	15	85	$Zn_4O(\mathbf{L^2})_{0.45}(\mathbf{L^3})_{2.55}$
MSO_2Me-36	25 : 75	36	64	$Zn_4O(\mathbf{L^2})_{1.08}(\mathbf{L^3})_{1.92}$
MSO_2Me-64	50 : 50	64	36	$Zn_4O(\mathbf{L^2})_{1.92}(\mathbf{L^3})_{1.08}$
MSO_2Me-79	75 : 25	79	21	$Zn_4O(\mathbf{L^2})_{2.38}(\mathbf{L^3})_{0.62}$
MSO_2Me-100	100 : 0	100	0	$Zn_4O(\mathbf{L^2})_3$
MSO_2Pr-100	-[c]	-	-	$Zn_4O(\mathbf{L^4})_3$

[a] As determined through ^{1}H NMR spectroscopy. [b]MSO_2Me-15 was synthesized starting from $H_2\mathbf{L^3}$ only. [c]MSO_2Pr-100 was synthesized starting from $H_2\mathbf{L^4}$ only.

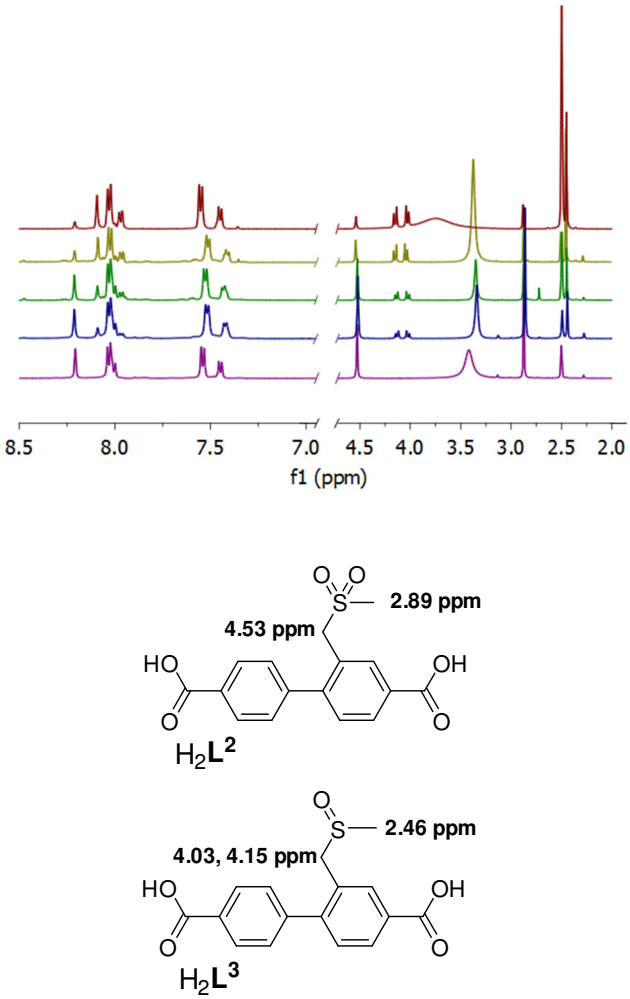

Figure 1. ^{1}H NMR spectra of digested samples of MSO_2Me-15 (red), MSO_2Me-36 yellow), MSO_2Me-64 (green), MSO_2Me-79 (blue), and MSO_2Me-100 (purple). The structures of $H_2\mathbf{L}^2$ and $H_2\mathbf{L}^3$ with key chemical shifts for the methyl and methylene protons indicated.

The crystallinity of the activated MOFs was analyzed by PXRD and the patterns are shown in Figure 2. Previously, MSO_2Me-100 was shown by SCXRD to have the doubly interpenetrated framework structure of IRMOF-9.[52] The MC-MOFs in this series all show peaks at identical 2θ positions and with similar intensities to activated MSO_2Me-100, signifying that all are isostructural with the interpenetrated IRMOF-9 structure type. After exposure to the atmosphere these patterns change quickly and eventually show no peaks, indicating poor stability of these MOFs towards atmospheric moisture. This has been

observed previously for MOFs with Zn_4O nodes[31] and for similarly functionalized frameworks.[53]

Additionally, MSO_2Pr-100 was analyzed by SCXRD. The framework crystallizes in the space group C2/*m*, as a pair of interpenetrated ***pcu*** frameworks. We and others have seen IRMOF-9-type structures crystallize in this space group with a variety of tagged biphenyl dicarboxylate (bpdc) ligands.[61-65] The sulfone tag groups were not located in the refinement due to both positional and dynamic disorder and the low resolution of the diffraction data. The PXRD pattern of MSO_2Pr-100 matches that calculated from the SCXRD structure and the other members of the series (Figure 2).

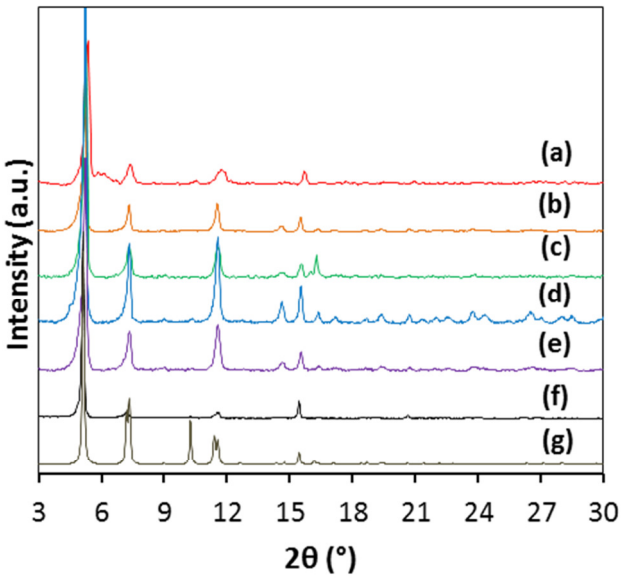

Figure 2. PXRD patterns of MSO_2Me-15 (a), MSO_2Me-36 (b), MSO_2Me-64 (c), MSO_2Me-79 (d), MSO_2Me-100 (e), MSO_2Pr-100 (f) and theoretical MSO_2Pr-100 (g).

The activated MOFs were analyzed by TG-DTA (Figure 3; Figures S9-S14). These show that 1-5 % of mass is lost below 100 °C. We attribute this to water being adsorbed during transfer and handling of the activated MOFs in air for a short time. Masses are maintained until approximately 235 °C, at which point the small mass losses observed are coupled with

exotherms, as indicated by peaks in the DTA response, the magnitude of which is related to the content of sulfoxide $\mathbf{L^3}$ linkers in the MC-MOFs. For MSO_2Me-15 we established the exotherm and mass loss corresponds to an elimination reaction of methanethiol from $\mathbf{L^3}$ to generate aldehyde groups and this process occurs for all the MC-MOFs here.[52-53] No exotherm or mass loss is observed for MSO_2Me-100 and MSO_2Pr-100 as these MOFs contain no $\mathbf{L^3}$. We have employed TG-DTA to detect post-synthetic reactions inside other MOFs.[62, 64, 66]

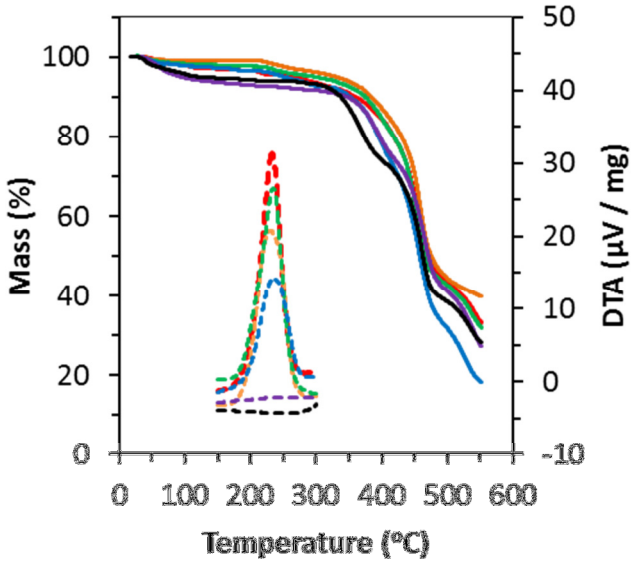

Figure 3. Full TG traces (solid lines) with partial inset DTA traces (dotted lines) for MSO_2Me-15 (red), MSO_2Me-36 (orange), MSO_2Me-64 (green), MSO_2Me-79 (blue), MSO_2Me-100 (purple) and MSO_2Pr-100 (black).

N_2 Gas Adsorption

In order to further characterize the MOFs, N_2 gas adsorption experiments at 77 K were carried out. All the MOFs show Type I isotherms (Figure 4a; Figures S15-S20) with relatively small variations in maximum adsorption, surface areas and pore volumes (Table 2). MSO_2Me-15 possesses the largest surface area, followed by MSO_2Me-64, with MSO_2Me-36, MSO_2Me-79 and MSO_2Me-100 having very similar surface areas. MSO_2Pr-100 displays a

smaller surface area than the other MOFs, due to the longer alkyl chain of the incorporated **L**[4] ligands. Pore size distributions from DFT analysis of the isotherm data indicate that MSO_2Me-15, MSO_2Me-36 and MSO_2Me-64 share pore sizes around 10 Å in diameter, while MSO_2Me-79, MSO_2Me-100 and MSO_2Pr-100 have slightly smaller, more narrowly distributed pores around 9.6 Å in diameter (Figure 4b). The accessible surface areas and pore size distributions are correlated with the slightly lower pore volumes of MSO_2Me-79 and MSO_2Me-100 and the lower values for MSO_2Pr-100.

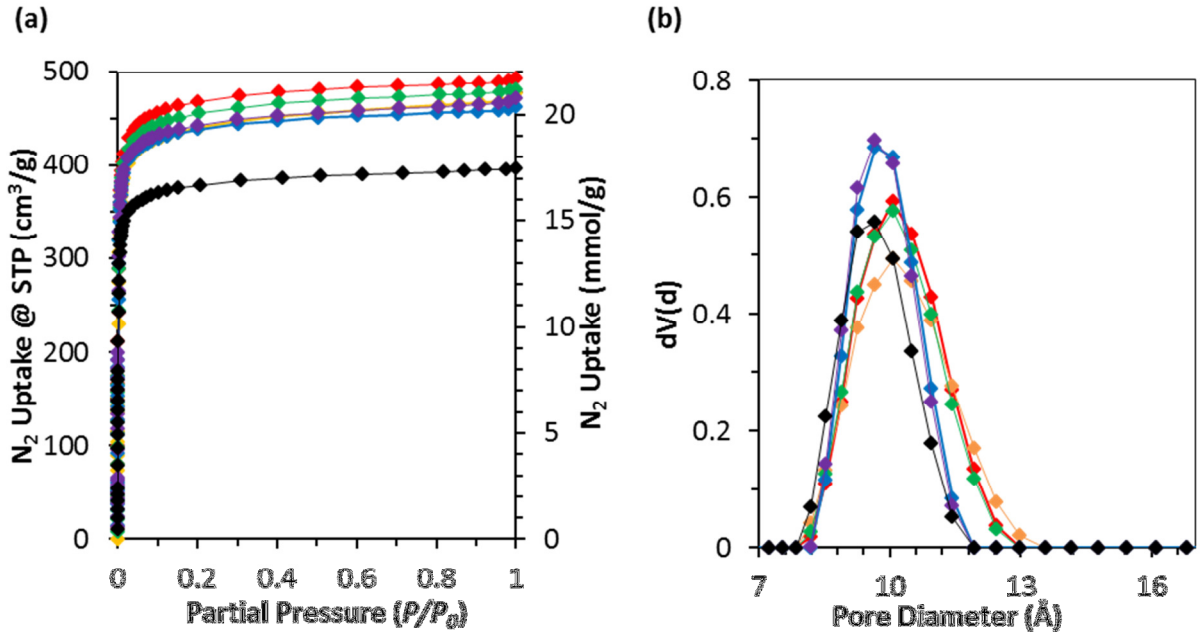

Figure 4. (a) N_2 adsorption isotherms at 77 K and (b) pore size distributions for MSO_2-15 (red), MSO_2Me-36 (orange), MSO_2Me-64 (green), MSO_2Me-79 (blue), MSO_2Me-100 (purple) and MSO_2Pr-100 (black).

Table 2. Characteristics of the MOFs derived from gas adsorption experiments

MOF	*Apparent BET Surface Area (m^2/g)* [a]	*N_2 Pore Volume (cm^3/g)* [b]	*CO_2/N_2 Selectivity at 298 K* [c]	*CO_2 Pore Volume (cm^3/g)* [d]
MSO_2Me-15	1888	0.73	13.1	0.82
MSO_2Me-36	1762	0.68	12.5	0.82

MSO_2Me-64	1827	0.70	11.1	0.79
MSO_2Me-79	1763	0.68	11.6	0.78
MSO_2Me-100	1776	0.69	14.2	0.78
MSO_2Pr-100	1514	0.59	21.9	0.65[e]

[a] BET analysis from N_2 adsorption at 77 K (see SI). [b] At P/P_0 0.20 and 77 K. [c] Obtained from IAST calculations for a mixture of 15% CO_2 and 85% N_2 (mole percent) at 298 K. [d] At 0.7 bar and 196 K. [e] At 0.6 bar and 196 K.

CO_2 Gas Adsorption

The CO_2 isotherms of each MOF were recorded at 196 K (Figure S22) and show equivalent uptake capacities to the N_2 isotherms at 77 K and only small differences in performance between the MOFs. MSO_2Me-15 and MSO_2Me-36 show increased CO_2 uptake over the other frameworks and this is most likely due to their slightly greater pore volumes (Table 2). However, MSO_2Me-100 and MSO_2Me-79 demonstrate increased CO_2 pore filling at lower pressures when compared with MSO_2Me-15, MSO_2Me-36 and MSO_2Me-64. MSO_2Pr-100 demonstrates similar CO_2 adsorption behavior albeit with a smaller maximum amount of adsorbed CO_2, in line with its lower accessible surface area.

The CO_2 adsorption properties of the MOFs were recorded at 273 K, 288 K and 298 K up to 1 bar (Figures S22-S27). The adsorption data at 298 K for all MOFs is shown in Figure 5a as a representative example. All samples show linear adsorption isotherms, with MSO_2Me-100 having the highest CO_2 adsorption capacity of all the samples and MSO_2Me-15, MSO_2Me-36, MSO_2Me-64 and MSO_2Pr-100 possessing similar CO_2 uptake capacities. This trend is consistent at each measurement temperature. MSO_2Me-100 and MSO_2Me-79 possess the highest capacities for CO_2. This is notable given these MOFs achieve greater CO_2 adsorption than other MC-MOFs with larger available pore space and surface area. Another notable result is that MSO_2Pr-100 achieves gravimetric CO_2 uptake comparable to MSO_2Me-

15 and MSO_2Me-64 despite a lower accessible surface area. Overall, the materials with the highest proportions of sulfone functionality possess the highest CO_2 capacities.

The enthalpy of CO_2 adsorption was calculated from isotherms recorded at 273, 288 and 298 K (Figure 5b). MSO_2Me-79 has an enthalpy of adsorption around 25 $kJmol^{-1}$ out to CO_2 loadings of 1 $mmolg^{-1}$. MSO_2Me-15, MSO_2Me-64, MSO_2Me-100 and MSO_2Pr-100 share similar enthalpies across all loadings (17-19 $kJmol^{-1}$) and MSO_2Me-36 displays a lower enthalpy across higher loadings of CO_2 (~15 $kJmol^{-1}$). These values are similar to dimethoxy, dihydroxyl and diiodo functionalized IRMOF-9 compounds.[67]

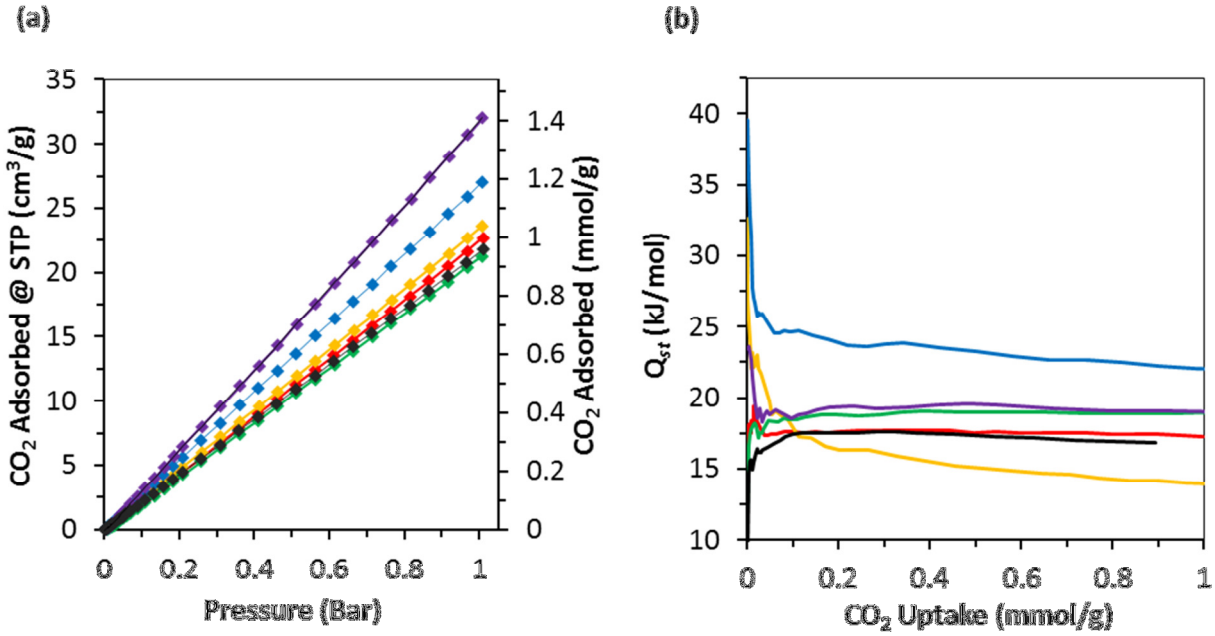

Figure 5. (a) CO_2 adsorption isotherms at 298 K and (b) enthalpy of CO_2 adsorption for MSO_2Me-15 (red), MSO_2Me-36 (orange), MSO_2Me-64 (green), MSO_2Me-79 (blue), MSO_2Me-100 (purple) and MSO_2Pr-100 (black).

IAST was used to calculate CO_2/N_2 selectivity factors at 298 K based on single-component CO_2 (Figure 5a) and N_2 (Figure S29) isotherms and a theoretical gas mixture of 15 mole percent CO_2 and 85 mole percent N_2 (Table 2; Figure S33).[68] The MOF with the highest selectivity factor was MSO_2Pr-100, followed by MSO_2Me-100, MSO_2Me-36, MSO_2Me-15, MSO_2-79 and finally MSO_2-64. The higher selectivity of MSO_2Pr-100 can be attributed to a

combination of good CO_2 adsorption performance and a reduction in N_2 adsorption (Figures S27-S28). The good performance of MSO_2Pr suggests the smaller pore size and more hydrophobic pore environment by incorporating the propyl group is favorable for selective CO_2 adsorption.

With regards to the MC-MOFs, there is no clear trend between the sulfoxide-sulfone ratio and selectivity factor. The CO_2/N_2 selectivities are comparable to other MOF materials. For example, the bpdc linked UiO-67 possesses two sizes of pores (11 Å and 8 Å diameter) and a selectivity of 9.4. However, incorporating a sulfone group into the bpdc linker is reported to increase the selectivity to 31.5.[16]

To observe performance at higher pressures, CO_2 isotherms were acquired at 298 K up to 10 bar (Figure S30) in which the MOFs all perform similarly with maximum uptakes between 170–200 cm^3/g. However, MSO_2Me-79 now outperforms MSO_2Me-100 in uptake capacity, and the isotherm of the latter shows some curvature indicating it is approaching saturation. Also notable is the good performance of MSO_2Pr-100 which shows an uptake capacity comparable to the higher surface area MOF, MSO_2Me-15.

Water Vapor Adsorption

The MOFs were analyzed for their water vapor adsorption properties at 298 K (Figure 6, Table 3). We were particularly interested in the performance for water adsorption given the mixture of polar functional groups. In previous work, sulfoxide-containing MOFs were shown to be more hydrophilic than their sulfone counterparts.[54] Frameworks in the IRMOF series tend to be hydrophobic and unstable to water.[32, 69-70]

The measured water isotherms are all of the same shape, with very little water uptake to approximately 0.4 P/P_0, then a broad step to a total uptake of 7 – 9 mmol/g. This type of adsorption curve is typical for hydrophobic MOFs,[71] and the step is thought to indicate the pressure at which water molecules cluster in the pores.[69]

MSO_2Me-15 shows the highest uptake of water vapor below 0.3 P/P_0, indicating water is more easily adsorbed into the pores compared with the other MOFs. On the other hand, MSO_2Pr-100 shows the least uptake in this range of all members in the series. Apart from MSO_2Me-36, all the MOFs undergo pore filling above 0.4 P/P_0. Changing the MC-MOF composition does not greatly affect the partial pressure at which the pore filling step occurs in these materials, as might be expected with having similar pore sizes and functional groups. It is notable that the MOF with the pore-filling step at the highest humidity is MSO_2Pr-100. We ascribe this to the increased hydrophobicity of the slightly smaller pores lined with the longer propyl tails. Additionally, all the MC-MOFs showed similar maximum water uptake of approximately 11 water molecules per formula unit (Table 3). These results are understandable given the similar hydrophilic properties of the sulfoxide and sulfone functional groups and the similar sizes of the pores in the MOFs.

The water isotherms show significant hysteresis and are not reversible. All the MOFs possess similar quantities of water remaining within their structures after desorption with a value of 2 molecules per formula unit (Table 3). These water molecules are likely to be binding to the metals in the structure, and it is known that Zn_4O nodes are capable of binding additional ligands.[61, 72-76] The collapse of the MOFs to non-porous amorphous materials after the water vapor isotherms was confirmed by CO_2 adsorption (Figure S31) and PXRD measurements (Figure S32). Considering many IRMOFs suffer similar collapse in contact with moisture, this is unsurprising.[31, 41, 53, 77]

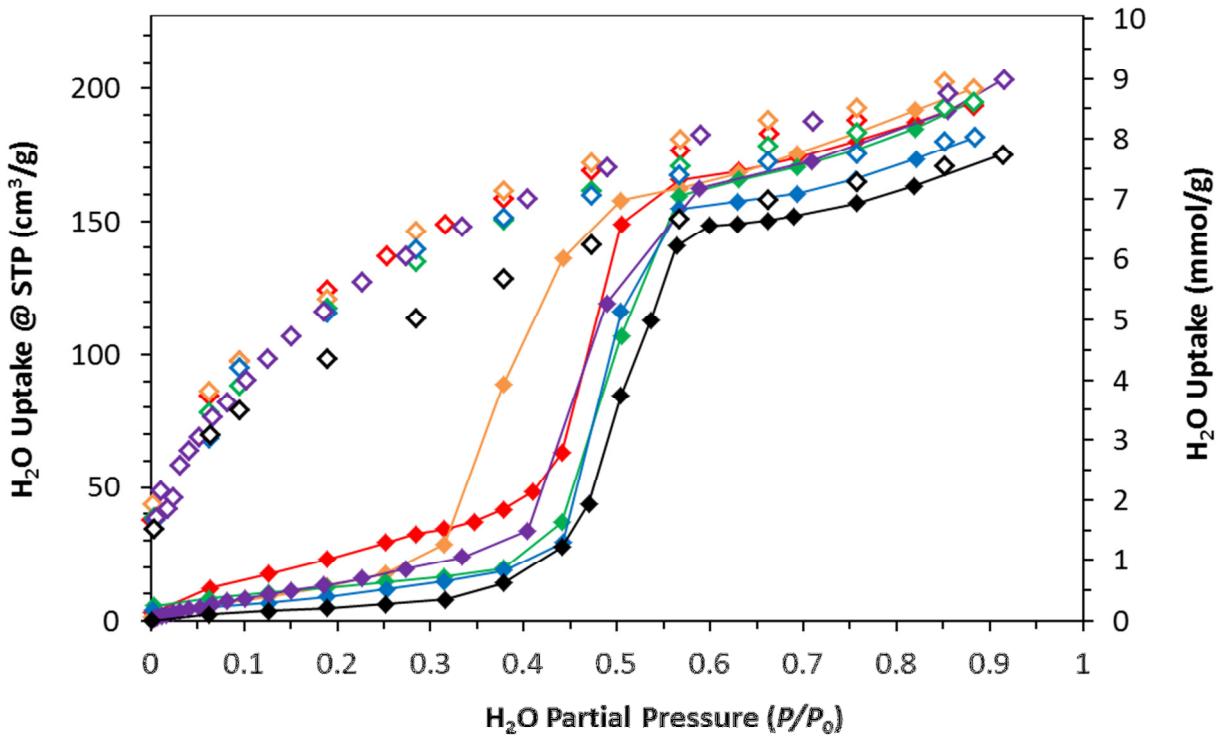

Figure 6. Water isotherms for MSO_2Me-15 (red), MSO_2Me-36 (orange), MSO_2Me-64 (green), MSO_2Me-79 (blue), MSO_2Me-100 (purple) and MSO_2Pr-100 (black). Adsorption as closed symbols, desorption as open symbols. Lines on the adsorption data provided as guides for the eye.

Table 3. Water uptake parameters of the MOFs at 298 K

MOF	*Total water uptake (mmol/g)*	*Water uptake in molecules per formula unit*[a]	*Water remaining post-sorption (mmol/g)*	*Water remaining in molecules per formula unit*
MSO_2Me-15	8.6	10.6	1.7	2.1
MSO_2Me-36	8.8	11.0	1.9	2.4
MSO_2Me-64	8.6	10.8	1.7	2.1
MSO_2Me-79	8.0	10.1	1.7	2.1

MSO_2Me-100	9.0	11.4	1.7	2.2
MSO_2Pr-100	7.7	10.5	1.5	2.0

[a] Formula unit based on framework formulations as in Table 1.

Conclusions

In summary, we have successfully synthesized a mixed-component IRMOF series with controlled ratios of sulfoxide and sulfone functionalities, in which the sulfoxide is obtained through *in situ* oxidation of a sulfide-containing ligand. This allowed us to systematically study the effects of ligand functionalization on gas and water adsorption properties of this isostructural set of MOFs. The surface areas of this set are consistent and compare favorably to other functionalized IRMOF-9 type frameworks.[64, 67] Overall, the best properties for CO_2 adsorption came from MOFs carrying greater proportions of the sulfone functionality. MSO_2Me-100 gave the greatest CO_2 uptake at 1 bar and MSO_2Pr-100 performed as well as MOFs with larger accessible surface areas and pore volumes. MSO_2Pr-100 gave the highest CO_2/N_2 selectivity which can be ascribed to a combination of pore constriction and increased hydrophobicity brought about by changing the sulfone alkyl chain from methyl to propyl. The enthalpies of CO_2 adsorption for the MC-MOF series range from 25-15 kJ mol^{-1} with the highest enthalpy shown by MSO_2Me-79. These results all demonstrate the fine tuning possible though a ligand-directed mixed-component approach.

The similar chemical functionality and pore diameters saw the water pore-filling step occur at roughly the same relative pressure for all the MC-MOFs, suggesting that the size of the pore is the primary parameter. However, changing the ligand tail from methyl to propyl pushed the pore filling step to higher humidity for MSO_2Pr-100.

In this series of functionalized IRMOF-9 compounds there are non-intuitive results. A complicating factor in the analysis is the subtleties of relative positioning and movements of the interpenetrated frameworks and associated functional groups upon activation and how

this contributes to their performance. Despite these complexities, the mixed-component strategy is worth pursuing in order to discover advanced MOF materials.

ASSOCIATED CONTENT

Supporting Information. ^{1}H and ^{13}C NMR spectra for $H_2\mathbf{L^4}$ and selected precursors, TG-DTA data, SCXRD data, PXRD patterns, gas sorption isotherms, information on surface area calculations, calculation results from IAST analysis. This material is available free of charge via the Internet at http://pubs.acs.org.

AUTHOR INFORMATION

Corresponding Author

* E-mail: chris_richardson@uow.edu.au

Author Contributions

The manuscript was written through contributions of all authors. All authors have given approval to the final version of the manuscript.

Funding Sources

The Science and Industry Endowment Fund, Australia. The Engineering and Physical Sciences Research Council (EPSCR), UK.

Notes

ACKNOWLEDGMENT

Parts of this work were supported by the Science and Industry Endowment Fund. ADB gratefully acknowledges support from the EPSRC (grant EP/H046305/1).

ABBREVIATIONS

bdc, benzene dicarboxylate; bpdc, 4,4′-biphenyl-dicarboxylate; bpy, 4,4′-bipyridine; DMF, *N,N′*-dimethylformamide; IAST, ideal adsorbed solution theory; IRMOF, isoreticular metal-organic framework; MC, mixed-component; MOF, metal-organic framework; UiO, University of Oslo; MIL, Materiaux de l'Institute Lavosier; NMR, nuclear magnetic resonance; PXRD, powder X-ray diffraction; SCXRD, single crystal X-ray diffraction; TG-DTA, thermogravimetric and differential thermal analysis; WUF, Wollongong University Framework;

REFERENCES

1. Yang, T.; Cui, H.; Zhang, C.; Zhang, L.; Su, C.-Y., *ChemCatChem* **2013,** *5*, 3131-3138.

2. Leus, K.; Liu, Y.-Y.; Van Der Voort, P., *Cat. Rev.* **2014,** *56*, 1-56.

3. Kreno, L. E.; Leong, K.; Farha, O. K.; Allendorf, M.; Van Duyne, R. P.; Hupp, J. T., *Chem. Rev.* **2012,** *112*, 1105-1125.

4. Couck, S.; Liu, Y.-Y.; Leus, K.; Baron, G. V.; Van der Voort, P.; Denayer, J. F. M., *Micropor. Mesopor. Mat.* **2015,** *206*, 217-225.

5. Mondloch, J. E.; Katz, M. J.; Isley III, W. C.; Ghosh, P.; Liao, P.; Bury, W.; Wagner, G. W.; Hall, M. G.; DeCoste, J. B.; Peterson, G. W.; Snurr, R. Q.; Cramer, C. J.; Hupp, J. T.; Farha, O. K., *Nat. Mater.* **2015,** *14*, 512-516.

6. Van de Voorde, B.; Bueken, B.; Denayer, J.; De Vos, D., *Chem. Soc. Rev.* **2014,** *43*, 5766-5788.

7. Zhang, M.; Bosch, M.; Gentle III, T.; Zhou, H.-C., *CrystEngComm* **2014,** *16*, 4069-4083.

8. Farha, O. K.; Hupp, J. T., *Acc. Chem. Res.* **2010,** *43*, 1166-1175.

9. Wu, C.-D.; Hu, A.; Zhang, L.; Lin, W., *J. Am. Chem. Soc.* **2005,** *127*, 8940-8941.

10. Ferguson, A.; Liu, L.; Tapperwijn, S. J.; Perl, D.; Coudert, F.-X.; Van Cleuvenbergen, S.; Verbiest, T.; van der Veen, M. A.; Telfer, S. G., *Nat. Chem.* **2016,** *8*, 250-257.

11. Gu, Z.-G.; Grosjean, S.; Brase, S.; Woll, C.; Heinke, L., *Chem. Commun.* **2015,** *51*, 8998-9001.

12. Burrows, A. D., Post-synthetic Modification of MOFs. In *Metal Organic Frameworks as Heterogeneous Catalysts*, Xamena, F. L. i.; Gascon, J., Eds. RSC: Cambridge, 2013; pp 31-75.

13. Meilikhov, M.; Yusenko, K.; Fischer, R. A., *J. Am. Chem. Soc.* **2009,** *131*, 9644-9645.

14. Gui, B.; Yee, K.-K.; Wong, Y.-L.; Yiu, S.-M.; Zeller, M.; Wang, C.; Xu, Z., *Chem. Commun.* **2015,** *51*, 6917-6920.

15. Lu, W.; Wei, Z.; Gu, Z.-Y.; Liu, T.-F.; Park, J.; Park, J.; Tian, J.; Zhang, M.; Zhang, Q.; Gentle III, T.; Bosch, M.; Zhou, H.-C., *Chem. Soc. Rev.* **2014,** *43*, 5561-5593.

16. Wang, B.; Huang, H.; Lv, X.-L.; Xie, Y.; Li, M.; Li, J.-R., *Inorg. Chem.* **2014,** *53*, 9254-9259.

17. Lammert, M.; Bernt, S.; Vermoortele, F.; De Vos, D. E.; Stock, N., *Inorg. Chem.* **2013,** *52*, 8521-8528.

18. Cook, T. R.; Zheng, Y.-R.; Stang, P. J., *Chem. Rev.* **2012,** *113*, 734-777.

19. Sumida, K.; Rogow, D. L.; Mason, J. A.; McDonald, T. M.; Bloch, E. D.; Herm, Z. R.; Bae, T.-H.; Long, J. R., *Chem. Rev.* **2011,** *112*, 724-781.

20. Li, J.-R.; Kuppler, R. J.; Zhou, H.-C., *Chem. Soc. Rev.* **2009,** *38*, 1477-1504.

21. D'Alessandro, D. M.; Smit, B.; Long, J. R., *Angew. Chemie Int. Ed.* **2010,** *49*, 6058-6082.

22. Das, A.; D'Alessandro, D. M., *CrystEngComm* **2015,** *17*, 706-718.

23. Yang, Q.; Wiersum, A. D.; Llewellyn, P. L.; Guillerm, V.; Serre, C.; Maurin, G., *Chem. Commun.* **2011,** *47*, 9603-9605.

24. Meek, S. T.; Teich-McGoldrick, S. L.; Perry, J. J.; Greathouse, J. A.; Allendorf, M. D., *J. Phys. Chem. C* **2012,** *116*, 19765-19772.

25. Biswas, S.; Zhang, J.; Li, Z.; Liu, Y.-Y.; Grzywa, M.; Sun, L.; Volkmer, D.; Van Der Voort, P., *Dalton Trans.* **2013,** *42*, 4730-4737.

26. Ko, N.; Hong, J.; Sung, S.; Cordova, K. E.; Park, H. J.; Yang, J. K.; Kim, J., *Dalton Trans.* **2015,** *44*, 2047-2051.

27. De Lange, M. F.; Gutierrez-Sevillano, J.-J.; Hamad, S.; Vlugt, T. J. H.; Calero, S.; Gascon, J.; Kapteijn, F., *J. Phys. Chem. C* **2013,** *117*, 7613-7622.

28. Han, S.; Huang, Y.; Watanabe, T.; Nair, S.; Walton, K. S.; Sholl, D. S.; Meredith, J. C., *Micropor. Mesopor. Mat.* **2013,** *173*, 86-91.

29. Jasuja, H.; Burtch, N. C.; Huang, Y.-g.; Cai, Y.; Walton, K. S., *Langmuir* **2012,** *29*, 633-642.

30. Yu, J.; Balbuena, P. B., *J. Phys. Chem. C* **2013,** *117*, 3383-3388.

31. Kaye, S. S.; Dailly, A.; Yaghi, O. M.; Long, J. R., *J. Am. Chem. Soc.* **2007,** *129*, 14176-14177.

32. Burtch, N. C.; Jasuja, H.; Walton, K. S., *Chem. Rev.* **2014,** *114*, 10575-10612.

33. Jasuja, H.; Jiao, Y.; Burtch, N. C.; Huang, Y.-g.; Walton, K. S., *Langmuir* **2014,** *30*, 14300-14307.

34. Schoenecker, P. M.; Carson, C. G.; Jasuja, H.; Flemming, C. J. J.; Walton, K. S., *Ind. Eng. Chem. Res.* **2012,** *51*, 6513-6519.

35. Liang, Z.; Marshall, M.; Chaffee, A. L., *Micropor. Mesopor. Mat.* **2010,** *132*, 305-310.

36. Fracaroli, A. M.; Furukawa, H.; Suzuki, M.; Dodd, M.; Okajima, S.; Gándara, F.; Reimer, J. A.; Yaghi, O. M., *J. Am. Chem. Soc.* **2014,** *136*, 8863-8866.

37. Deria, P.; Mondloch, J. E.; Tylianakis, E.; Ghosh, P.; Bury, W.; Snurr, R. Q.; Hupp, J. T.; Farha, O. K., *J. Am. Chem. Soc.* **2013,** *135*, 16801-16804.

38. Yu, C.; Bourrelly, S.; Martineau, C.; Saidi, F.; Bloch, E.; Lavrard, H.; Taulelle, F.; Horcajada, P.; Serre, C.; Llewellyn, P. L.; Magnier, E.; Devic, T., *Dalton Trans.* **2015,** *44*, 19687-19692.

39. Noro, S.-i.; Matsuda, R.; Hijikata, Y.; Inubushi, Y.; Takeda, S.; Kitagawa, S.; Takahashi, Y.; Yoshitake, M.; Kubo, K.; Nakamura, T., *ChemPlusChem* **2015,** *80*, 1517-1524.

40. Cmarik, G. E.; Kim, M.; Cohen, S. M.; Walton, K. S., *Langmuir* **2012,** *28*, 15606-15613.

41. Nguyen, J. G.; Cohen, S. M., *J. Am. Chem. Soc.* **2010,** *132*, 4560-4561.

42. Liu, L.; Telfer, S. G., *J. Am. Chem. Soc.* **2015,** *137*, 3901-3909.

43. Zhang, Y.-B.; Furukawa, H.; Ko, N.; Nie, W.; Park, H. J.; Okajima, S.; Cordova, K. E.; Deng, H.; Kim, J.; Yaghi, O. M., *J. Am. Chem. Soc.* **2015,** *137*, 2641-2650.

44. Burrows, A. D., *CrystEngComm* **2011,** *13*, 3623-3642.

45. Burrows, A. D.; Fisher, L. C.; Richardson, C.; Rigby, S. P., *Chem. Commun.* **2011,** *47*, 3380-3382.

46. Deng, H.; Doonan, C. J.; Furukawa, H.; Ferreira, R. B.; Towne, J.; Knobler, C. B.; Wang, B.; Yaghi, O. M., *Science* **2010,** *327*, 846-850.

47. Khutia, A.; Rammelberg, H. U.; Schmidt, T.; Henninger, S.; Janiak, C., *Chem. Mater.* **2013,** *25*, 790-798.

48. Reinsch, H.; Waitschat, S.; Stock, N., *Dalton Trans.* **2013,** *42*, 4840-4847.

49. Horike, S.; Inubushi, Y.; Hori, T.; Fukushima, T.; Kitagawa, S., *Chem. Sci.* **2012,** *3*, 116-120.

50. Yang, J.; Grzech, A.; Mulder, F. M.; Dingemans, T. J., *Eur. J. Inorg. Chem.* **2013,** *13*, 2336-2341.

51. Park, T.-H.; Koh, K.; Wong-Foy, A. G.; Matzger, A. J., *Cryst. Growth Des.* **2011,** *11*, 2059-2063.

52. Burrows, A. D.; Frost, C. G.; Mahon, M. F.; Richardson, C., *Chem. Commun.* **2009**, 4218-4220.

53. Bryant, M. R.; Richardson, C., *CrystEngComm* **2015,** *17*, 8858-8863.

54. Wade, C. R.; Corrales-Sanchez, T.; Narayan, T. C.; Dinca, M., **2013,** *6*, 2172-2177.

55. Halis, S.; Reimer, N.; Klinkebiel, A.; Lüning, U.; Stock, N., *Micropor. Mesopor. Mat.* **2015,** *216*, 13-19.

56. Neofotistou, E.; Malliakas, C. D.; Trikalitis, P. N., *Chem. Eur. J.* **2009,** *15*, 4523-4527.

57. Julian, H.; Wenten, I. G., *IOSR JE* **2012,** *2*, 484-495.

58. Weigang Lu; Daqiang Yuan; Julian Sculley; Dan Zhao; Rajamani Krishna; Zhou, H.-C., *J. Am. Chem. Soc.* **2011,** *133*, 18126-18129.

59. FSProcess. Rigaku Corporation: Tokyo, Japan, 1996.

60. Sheldrick, G., *Acta Cryst. A* **2008,** *64*, 112-122.

61. Burrows, A. D.; Frost, C. G.; Mahon, M. F.; Richardson, C., *Angew. Chemie Int. Ed.* **2008,** *47*, 8482-8486.

62. Ablott, T. A.; Turzer, M.; Telfer, S. G.; Richardson, C., *Cryst. Growth Des.* **2016,** *16*, 7067-7073.

63. Rankine, D.; Avellaneda, A.; Hill, M. R.; Doonan, C. J.; Sumby, C. J., *Chem. Commun.* **2012,** *48*, 10328-10330.

64. Burrows, A. D.; Hunter, S. O.; Mahon, M. F.; Richardson, C., *Chem. Commun.* **2013,** *49*, 990-992.

65. Roberts, J. M.; Farha, O. K.; Sarjeant, A. A.; Hupp, J. T.; Scheidt, K. A., *Cryst. Growth Des.* **2011,** *11*, 4747-4750.

66. Tshering, L.; Hunter, S. O.; Nikolich, A.; Minato, E.; Fitchett, C. M.; D'Alessandro, D. M.; Richardson, C., *CrystEngComm* **2014,** *16*, 9158-9162.

67. Babarao, R.; Coghlan, C. J.; Rankine, D.; Bloch, W. M.; Gransbury, G. K.; Sato, H.; Kitagawa, S.; Sumby, C. J.; Hill, M. R.; Doonan, C. J., *Chem. Commun.* **2014,** *50*, 3238-3241.

68. Simon, C. M.; Smit, B.; Haranczyk, M., *Comput. Phys. Commun.* **2016,** *200*, 364-380.

69. De Toni, M.; Jonchiere, R.; Pullumbi, P.; Coudert, F.-X.; Fuchs, A. H., *ChemPhysChem* **2012,** *13*, 3497-3503.

70. Canivet, J.; Fateeva, A.; Guo, Y.; Coasne, B.; Farrusseng, D., *Chem. Soc. Rev.* **2014,** *43*, 5594-5617.

71. Küsgens, P.; Rose, M.; Senkovska, I.; Fröde, H.; Henschel, A.; Siegle, S.; Kaskel, S., *Micropor. Mesopor. Mat.* **2009,** *120*, 325-330.

72. Hausdorf, S.; Wagler, J. r.; Moβig, R.; Mertens, F. O. R. L., *J. Phys. Chem. A* **2008,** *112*, 7567-7576.

73. Schrock, K.; Schroder, F.; Heyden, M.; Fischer, R. A.; Havenith, M., *Phys. Chem. Chem. Phys.* **2008,** *10*, 4732-4739.

74. Akimbekov, Z.; Wu, D.; Brozek, C. K.; Dinca, M.; Navrotsky, A., *Phys. Chem. Chem. Phys.* **2016,** *18*, 1158-1162.

75. Bellarosa, L.; Brozek, C. K.; García-Melchor, M.; Dincă, M.; López, N., *Chem. Mater.* **2015,** *27*, 3422-3429.

76. Greathouse, J. A.; Allendorf, M. D., *J. Am. Chem. Soc.* **2006,** *128*, 10678-10679.

77. Bury, W.; Justyniak, I.; Prochowicz, D.; Wrobel, Z.; Lewinski, J., *Chem. Commun.* **2012,** *48*, 7362-7364.

For Table of Contents Only

Mixed-component sulfone–sulfoxide tagged zinc IRMOFs: In situ ligand oxidation, carbon dioxide and water sorption studies

Macguire R. Bryant, Andrew D. Burrows, Cameron J. Kepert, Peter D. Southon, Omid T. Qazvini, Shane G. Telfer, and Christopher Richardson

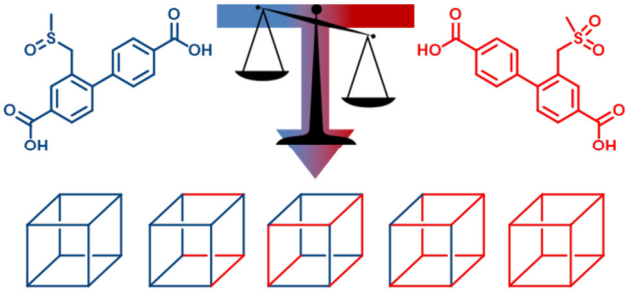

A multi-component zinc IRMOF series has been prepared via a novel *in situ* reaction to give alkyl-tailed sulfoxide and sulfone tag groups. The gas and water adsorption properties of the resulting isostructural set of MOFs were investigated. MOFs with higher proportions of sulfone groups had better CO_2 adsorption characteristics while MOFs with longer alkyl tails pushed the pore-filling step in water adsorption isotherms to higher humidity.